The effect of inflation on the morphology-derived rheological parameters of lava flows and its implications for interpreting remote sensing data - A case study on the 2014/2015 eruption at Holuhraun, Iceland

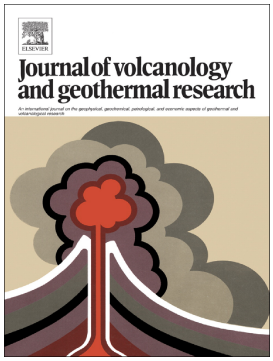

The effect of inflation on the morphology-derived rheological parameters of lava flows and its implications for interpreting remote sensing data - A case study on the 2014/2015 eruption at Holuhraun, Iceland

S. Kolzenburg, J. Jaenicke, U. Münzer, D.B. Dingwell

PII: S0377-0273(17)30520-6
DOI: doi:10.1016/j.jvolgeores.2018.04.024
Reference: VOLGEO 6367

To appear in: *Journal of Volcanology and Geothermal Research*

Received date: 17 August 2017
Revised date: 8 February 2018
Accepted date: 25 April 2018

Please cite this article as: S. Kolzenburg, J. Jaenicke, U. Münzer, D.B. Dingwell , The effect of inflation on the morphology-derived rheological parameters of lava flows and its implications for interpreting remote sensing data - A case study on the 2014/2015 eruption at Holuhraun, Iceland. The address for the corresponding author was captured as affiliation for all authors. Please check if appropriate. Volgeo(2017), doi:10.1016/j.jvolgeores.2018.04.024

The effect of inflation on the morphology-derived rheological parameters of lava flows and its implications for interpreting remote sensing data.

- A case study on the 2014/2015 eruption at Holuhraun, Iceland -

S. Kolzenburg[1,3], J. Jaenicke[2], U. Münzer[2], D.B. Dingwell[1]

Department of Earth and Environmental Sciences

Section for Mineralogy, Petrology and Geochemistry (1)

Section Geology (2)

Ludwig-Maximilians-Universität

80333 Munich, Germany

Department of Earth and Planetary Sciences (3)

McGill University

H3A 0E8 Montreal, Quebec, Canada

Submitted to:

JVGR

Corresponding author: Stephan Kolzenburg; skolzenburg@gmail.com

Keywords: Lava flow; Morphology; Rheology; Planetary Volcanism; Holuhraun

Abstract

Morphology-derived lava flow rheology is a frequently used tool in volcanology and planetary science to determine rheological parameters and deduce the composition of lavas on terrestrial planets and their moons. These calculations are usually based on physical equations incorporating 1) lava flow driving forces: gravity, slope and flow-rate and 2) morphological data such as lava flow geometry: flow-width, -height or shape of the flow outline. All available methods assume that no geometrical changes occur after emplacement and that the measured flow geometry reflects the lava's apparent viscosity and/or yield strength during emplacement. It is however well-established from terrestrial examples that lava flows may inflate significantly after the cessation of flow advance. This inflation affects, in turn, the width-to-height ratio upon which the rheological estimates are based and thus must result in uncertainties in the determination of flow rheology, as the flow height is one of the key parameters in the morphology-based deduction of flow properties. Previous studies have recognized this issue but, to date, no assessment of the magnitude of this error has been presented. This is likely due to a lack of digital elevation models (DEMs) at sufficiently high spatial and temporal resolution.

The 2014/15 Holuhraun eruption in central Iceland represents one of the best monitored large volume (1.5 km^3) lava flow fields (85 km^2) to date. An abundance of scientific field and remote sensing data were collected during its emplacement. Moreover, inflation plays a key role in the emplacement dynamics of the late stage of the lava field. Here, we use a time series of high resolution DEMs acquired by the TanDEM-X satellite mission prior, during and after the eruption to evaluate the error associated with the most common methods of deriving lava flow rheology from morphological parameters used in planetary science.

We can distinguish two dominant processes as sources of error in the determination of lava flow rheology from morphology 1) wholesale inflation of lava channels and 2) post halting inflation of individual lava toes. These result in a 2.4- to 17 - fold overestimation of apparent viscosity and a 0.7- to 2.4 - fold overestimation of yield strength. When applied in planetary sciences, this overestimation in rheological parameters translates directly to an overestimation of the respective lavas silica content. We conclude that, although qualitatively informative, morphological analysis is insufficient to discern lava rheology and composition. Instead, *in-situ* analysis together with high resolution remote sensing data is needed to properly constrain the compositions involved in planetary volcanism.

1. Introduction

The rheology and composition of lava flows observed on other planets is commonly estimated from the morphology of lava flows (Baloga et al., 2003; Glaze and Baloga, 2006; Glaze et al., 2003; Hulme, 1974; Moore et al., 1978; Warner and Gregg, 2003; Wilson and Head, 1994). These approaches have been developed and tested on analogue materials (Gregg and Fink, 2000; Griffiths and Fink, 1992; Pinkerton and Wilson, 1994). The individual approaches including all input parameters and limitations are discussed in detail in section 3 of this manuscript. Deducing flow properties from the 3D-shape of lava flows is a useful tool to establish paleo-emplacement conditions of lava flows on both Earth and other terrestrial planets and their satellites, informing estimates of the variability of compositions of lavas on planets where direct measurements are lacking (Baloga et al., 2003; Bruno et al., 1994; Chevrel et al., 2013b; Glaze et al., 2003; Hiesinger et al., 2007; Hulme and Fielder, 1977; Keszthelyi et al., 2006; Moore et al., 1978; Warner and Gregg, 2003; Wilson and Head, 1994; Zimbelman, 1985).

Such deductions of flow parameters from geometric measurements are obtained from static post-emplacement morphologies and must therefore be seen to be a cumulative result of the entire deformational history of the flow during emplacement. Inferring rheological parameters such as viscosity and/or yield strength from post-emplacement flow morphology is, therefore, based on a number of assumptions, namely: 1) the rheology did not change during emplacement (Hiesinger et al., 2007; Hulme, 1974; Moore et al., 1978), 2) the geometry is representative of the lava at flow conditions (Glaze and Baloga, 2006; Glaze et al., 2003; Hulme, 1974; Pasckert et al., 2012; Warner and Gregg, 2003; Wilson and Head, 1994), and 3) the lava is emplaced as a single coherent isothermal flow (Baloga et al., 2001; Baloga et al., 2003; Glaze et al., 2003; Moore et al., 1978).

Direct observations of lava flow dynamics on earth show that these assumptions are significant simplifications of lava flow emplacement processes. Firstly, lava flows undergo continuous changes in rheology during emplacement (Cashman et al., 2013; Cashman et al., 1999; Chevrel et al., 2013b; Decker et al., 1987; Giordano et al., 2007; Kolzenburg et al., 2016b; Kolzenburg et al., 2017). Secondly, lava flow geometry may change significantly during emplacement and lava flows often inflate after reaching their final runout distance (Cashman et al., 2013; Hon et al., 1994; Pedersen et al., 2017; Walker, 1991). Thirdly, lava flows are often emplaced in a non-continuous and pulsating manner (Cashman et al., 2013; Favalli et al., 2010; Kolzenburg et al., 2017; Pedersen et al., 2017).

Application and interpretation of morphological methods for the determination of rheological parameters from post-emplacement geometries thus need to be reviewed in the light of the effects that all the above-mentioned processes may have on the results obtained. Some estimates of the effects of changing rheology and densification through gas loss on flow

thickness have been presented in a theoretical approach by Baloga et al. (2001). The model is based on the aforementioned assumptions of flow emplacement and does not account for natural emplacement processes such as inflation. They show that even under those assumptions calculated changes in lava flow height due to different densities and viscosities may be up to 40%, depending on model input parameters.

The main issue hampering the correlation of rheology and morphology is that lava flows display complex emplacement dynamics that commonly feature a two-phase emplacement mechanism (independent of surface textures). An initial free-flow stage, where rheology can readily be deduced from the gravitational forcing of the lava as a function of density and slope of the emplacement surface (see Hiesinger et al. (2007) and Chevrel et al. (2013b) for reviews) and a subsequent inflation stage, where the lava flow is self-confined by a growing rheological contrast zone or "crust". Although flow advance may continue to a certain degree, mainly in pāhoehoe type flows (Hon et al., 1994), the areal extent of the lava no longer increases significantly during the inflation stage. Instead newly erupted lava is accommodated via flow inflation and its height may increase by a factor of up to 10 (Cashman et al., 2013; Hon et al., 1994; Pedersen et al., 2017; Walker, 1991). This process will result in estimates of lava viscosity and yield strength higher than the actual values during flow. Thus it becomes apparent that assigning a geometry-derived yield strength to a lava is extremely problematic. This is because the lava flow height is controlled by the confinement of the developing flow-carapace (i.e. external confinement by the rheologic contract zone) rather than an apparent internal yield-strength (intrinsic rheologic parameter). It is important to note that in nature, even the fluid core of a lava flow is not actually a Bingham fluid but, being a three phase magmatic suspension, has a complex, strain-rate-dependent viscosity. The crust on the other hand contains brittle and

visco-elastic portions. Therefore, the use of a Bingham rheology model represents a drastic simplification and is a significant source of uncertainty and error in the estimation of flow properties from morphology, since height is a second to fourth power parameter in the respective equations (See section 3 for details).

Here, for the first time, use of a time series of high resolution remote sensing elevation data (morphology and texture) recorded by the TanDEM-X satellite mission during the 2014/15 Holuhraun eruption in Iceland enables the systematic assessment of the influence of lava flow inflation on the results obtained from current methods for the derivation of rheology from morphology.

2. Geological Setting and Eruption Chronology

The Holuhraun eruption took place in the tectonic fissure swarm between the Bárðarbunga-Veiðivötn and the Askja volcanic systems in the periglacial sander plain of Dyngjujökull, an outlet glacier of the Vatnajökull ice cap in Iceland (Fig. 1). It was fed by a 45 km long, lateral dyke propagating from the subglacial Bárðarbunga volcano (Coppola et al., 2017; Ruch et al., 2016; Sigmundsson et al., 2014). The eruption lasted about six months (29/08/2014 – 27/02/2015) and produced about 1.5 km^3 of basaltic lava (Coppola et al., 2017; Jaenicke et al., 2014; Jaenicke et al., 2016; Münzer et al., 2016; Pedersen et al., 2017). The lava flow extends over an area of 85 km^2 with a maximum height of 48 m of the main crater (Baugur) located at the southwestern edge of the lava field (Jaenicke et al., 2014; Jaenicke et al., 2016; Münzer et al., 2016; Pedersen et al., 2017). The large volume and area of the Holuhraun flow-field makes it a great comparative counterpart to extra-terrestrial flow-fields such as King- and Aristarchus-Crater on moon (Moore et al., 1978) and Olympus-, Arisa- and Ascrae-Mons on Mars (Moore et al., 1978; Zimbelman, 1985).

Lava effusion rates during the eruption period range from 320 to 10 m^3/s. Averaged values are ~250, 100 and 50 m^3/s during the initial (August – September 2014), intermediate (October – December 2014) and final phase (December 2014 to February 2015), respectively (Coppola et al., 2017; Pedersen et al., 2017). The lava was emplaced on the central part of the Flæður floodplain north of the Dyngjujökull glacier. This outwash plain is covered by glacial and fluvial deposits, and has a regional dip of ~0.2°-0.5° to the northeast. Its small scale topography is made of decimeter to meter scale fluvial banks, bars and terraces. The gently sloping emplacement surface resulted in slow lava flow advancement rates (generally below ~1 m/min); see , Kolzenburg et al. (2017) and Pedersen et al. (2017) for details. Thus the eruption was an ideal target for scientific observations of unique detail ranging from direct ground measurements (Kolzenburg et al., 2017; Pedersen et al., 2017) over airborne platforms to satellite monitoring (Coppola et al., 2017; Jaenicke et al., 2014; Jaenicke et al., 2016; Münzer et al., 2016; Pedersen et al., 2017). The chemical composition of the lava is homogeneous throughout the entire eruption (Gíslason et al., 2015; Kolzenburg et al., 2017). This implies that neither the topography nor the composition were the driving factors for the observed changes in flow morphology.

During its emplacement history, the lava field was initially dominated by channels and horizontal expansion. Then it transitioned to grow in volume primarily by inflation, tube-fed flow (i.e. transport of lava through roofed over partially or completely filled channels) and vertical stacking of lava-lobes. The main lava channel shows significant inflation (5-10 m). Inflation intensity increases from proximal to distal sections of the lava channel, see Pedersen et al. (2017) and section 5 for details. Pedersen et al. (2017) estimated a total lava volume of 0.09 km^3 to 0.18 km^3 (i.e. about 10% of the erupted lava volume) to produce such inflation.

As highlighted in Pedersen et al. (2017), the Holuhraun flow field illustrates that studies of long-lived eruptions based exclusively on the final surface morphology may be incapable of revealing the complex morphological evolution of composite lava-fields. Here, the high spatial and temporal resolution of monitoring data available for the Holuhraun eruption provides a unique opportunity to study the emplacement and the growth of a large, composite lava flow field in both space and time. This is crucial for the assessment of errors resulting from geometrical changes during and post-emplacement, a fundamental part being the availability of sequential DEMs of the lava flow-field.

3. Brief Review of Existing Methods

The most commonly used methods for the determination of rheological parameters from lava flow morphology can broadly be separated into two groups: 1) Methods estimating the apparent viscosity of the lava through the relationships between flow-geometry (width, height), flow-rate (surface velocity or volumetric flux) and flow-driving forces (gravity, lava-density, and slope) and 2) Methods estimating the yield strength of the lava based on flow-geometry (width, height) and flow-driving forces (gravity, lava-density, and slope). These methods neglect the volumetric flow rate by assuming a constant Bingham rheology, where the final width to height ratio of the lava directly correlates with its yield strength.

Other, less commonly applied approaches include fractal analysis of the flow outlines (Bruno et al., 1994), analysis of flow thickness along the longitudinal axis of the flow (Glaze et al., 2003) or rate of levee growth along the flow (Glaze and Baloga, 2006). In this study we focus on the evaluation of the first two groups of methods, as these are the most commonly applied approaches in planetary sciences.

In order to apply these methods it is necessary to constrain the volumetric flux of lava for the eruption in question. Several approaches for doing so have been proposed for cooling-limited, laminar lava flows. Inflation, however, is neglected in such calculations. These approaches relate lava flow length to flow velocity via the dimensionless Graetz number; see Pinkerton and Wilson (1994) and references therein, which considers the relationship between heat advection to conductive heat loss along the lava flow length as follows:

$$G_z = \frac{v\, d_e^2}{k\, l} \qquad \text{eq. 1}$$

Where G_z is the Graetz number, v the mean flow velocity in m/s, d_e the equivalent diameter of the flow in meters, k the thermal diffusivity in m^2s^{-1} and l the lava flow length in meters. Cooling limited lava flows have been found to stop once this number falls to a critical value of 300 (Pinkerton and Wilson, 1994). This Graetz number threshold as well as the flow dimensions are correlated to the volumetric effusion rate; see Chevrel et al. (2013b) for a review:

$$Q = u\, w\, h = \frac{G_z\, k\, l\, w}{h} \qquad \text{eq. 2}$$

Group 1 approaches (i.e. determination of the viscosity of the lava) rely on information about the mean flow velocity of lava along the investigated channel. They are commonly based on the Jeffreys equation. Nichols (1939) developed the Jeffreys equation into an approach that can be applied to lava flow emplacement:

$$\eta_1 = \frac{g\, sin\alpha\, h^2 \rho}{n\, v} \qquad \text{eq. 3}$$

Where η_1 is the viscosity in Pa s, ρ is the lava density in kg/m^3, α is the angle of the underlying slope in degrees, h is the lava flow height in meters and n is a constant set to 4 for narrow flows.

The mean flow velocity v is related to the channel geometry and effusion rate via equation 2, above. Nichols' equation can therefore, when accounting for flow geometry and assuming Newtonian viscosity, be re-written as:

$$\eta_2 = \frac{\rho\, g\, h^3\, w\, sin\alpha}{n\, Q} \qquad \text{eq. 4}$$

where all parameters are as defined above. Based on the work of Fink and Griffiths (1990), this equation was simplified by Warner and Gregg (2003) to derive the effective bulk viscosity of crust forming lavas independent of flow width:

$$\eta_3 = \frac{\rho\, g\, h^4}{Q} \qquad \text{eq. 5}$$

Group 2 approaches are based on the assumption of lava having a Bingham rheology, i.e. a yield strength forcing the flow to stop at a critical slope, thereby determining its geometry, which is recorded in the solidified flow. Relating yield strength to geometry was initially proposed by Hulme (1974) and developed into three separate equations presented in Moore et al. (1978):

$$\tau_1 = \rho\, g\, h\, sin\alpha \qquad \text{eq. 6}$$

$$\tau_2 = \frac{\rho\, g\, h^2}{w} \qquad \text{eq. 7}$$

$$\tau_3 = \rho\, g \sin^2\alpha\, 2w_l \qquad \text{eq. 8}$$

Where w_l is the levee width and all other parameters are equivalent to the previous equations. Equation 6 simply balances the driving forces (density, height slope) and gravity. Equation 7 is slope independent, only assessing the lateral spreading of the flow, and was originally developed by Orowan (1949); derived from the flow of glaciers as analogues. This equation is also used in Zimbelman (1985) and allows to deduce yield strength without knowing the gradient of the underlying slope by restricting calculations to the lateral spreading of the lava flow perpendicular to the flow axis. Equation 8 accounts for the development of flow directing levees and is therefore commonly used for channelized flows.

In the following analysis we focus on equations 4, 5, 6 and 7 since all input parameters are well-constrained for these approaches. Equation 8 is not assessed because, due to the inflation and overflow events that infilled the channels during emplacement, it was not possible to constrain the modifications in channel width satisfactorily.

4. Satellite Elevation Data

Within the framework of the project IsViews (Iceland subglacial Volcanoes interdisciplinary early warning system, 2012-2016) radar data were recorded by the TerraSAR-X and TanDEM-X satellites during the Holuhraun eruption. A Geomorphometric analysis using the TXD data is presented in Dirscherl and Rossi (2018). These data are property of the DLR and were made available for this study in the framework of a collaborative project (IsViews, Proposal Other 2375, PI. C. Minet). In addition, very high resolution (20 cm), UltraCam Xp data (Gruber et al., 2008; Wiechert et al., 2011) were acquired on 29/08/2014 (start of the eruption) and 08/09/2015 to interpret the exact outline of the lava field on a processed true orthophoto mosaic and for verification the TDX data. Albeit higher 3D-resolution may be recovered by laser scanning or photogrammetry (Cashman et al., 2013; Farquharson et al., 2015; Kolzenburg et al., 2016a),

these methods can only be deployed locally and are, to date, unable to cover the large spatial extent represented by the Holuhraun lava-field in a satisfactory time-frame. The advantage of radar technology, especially in view of the frequent cloudy conditions in Iceland, is its ability to collect data independent of solar illumination and cloud cover.

TanDEM-X (TerraSAR-X add-on for Digital Elevation Measurement) is the name of TerraSAR-X's twin satellite, a German Earth observation satellite using X-band SAR (Synthetic Aperture Radar). The TanDEM-X mission has been established in 2010 with the aim to generate a global digital elevation model (DEM) at 12 m posting using interferometric SAR (InSAR) technique (Krieger et al., 2007; Münzer et al., 2010). Additionally, the mission operation allows stacks of bistatic acquisitions (pairs of Coregistered Single look Slant range Complex; CoSSC's) within the framework of science proposals in order to generate temporal DEM series (Hajnsek and Busche, 2015).

TanDEM-X (TDX) elevation data with a ground resolution of 6 m, acquired before (22/01/2011), during (06/12/2014, 10/02/2015) and after (28/04/2015) the Holuhraun eruption, were available for this study. The acquisitions were processed as RawDEMs at the German Aerospace Centre (DLR) using the operational Integrated TanDEM-X Processor (ITP) (Rossi et al., 2012). The individual RawDEMs each represent a single time and thus can be used to investigate temporal height changes. Within a time-series of TDX RawDEMs of the same orbit absolute height differences between DEMs are common (Mayer et al., 2016; Münzer et al., 2016; Rossi et al., 2016). Therefore, surface elevation change is derived by means of DEM differencing using precisely co-registered TDX DEM data. Since we analyse topographical changes relative to one of the acquisitions in the data stack, the flat and solid terrain around the lava flow could be used for calibration to a master scene (28/04/2015). According to height error maps provided by

the DLR, the vertical accuracy of the TDX data within the investigated area is ~20 cm. However, the extreme heat (up to 1200℃) of the lava yields to artefacts that need to be considered when interpreting the TDX data acquired during the Holuhraun eruption. These artefacts were identified in the TDX data from 06/12/2014. There are two types of errors: 1) "Wave patterns" due to atmospheric heat propagating with the wind westwards from the main crater (Figure 2B) and 2) "local scatter" of the radar backscatter at active flow fronts where the lava is glowing (Figure 2D and Figure 3). Landsat 8 data from USGS, acquired during the eruption, were used in order to verify these occurrences.

5. Identification of Target Areas

During the Holuhraun eruption two emplacement processes caused most of the modifications to the lava flow geometry:

1. Inflation of lava channels or tubes that were created during a constant flow regime and then later experienced increased internal pressure via either an increased volume flux or pressure tailback (i.e. pressure increase when downstream flow is blocked or confined); Figure 2B.
2. Inflation of individual flow lobes via formation of a flow-confining crust that stopped flow advance and was subsequently inflated to accommodate the continued arrival of lava; Figure 2D.

We processed difference TDX DEMs for the time periods between all available datasets to assess the relative changes in the lava flow-field (see Fig. 2). These were used to identify target areas for the investigation of the different inflation mechanisms, and to assess the respective impact on the morphology derived rheologic parameters. Representative elevation profiles of single TDX DEMs of these areas were then generated in order to quantify the

morphological readings used in the calculation of the lavas' rheological parameters. In the following sections we detail how the target areas were chosen for investigation of the respective process.

5.1 Zones for Application of the Standard Method

For comparison to the results of areas where inflation was identified, we selected areas where emplacement occurred as a single unit and without identifiable post-emplacement modifications (Fig. 2A). These areas may have been inflated during late stages of flow (see section 5.3) but were free of secondary inflation. Due to the nature of the eruption (including several periods of re-activation of old parts of the flow field and superposition of flow units), single stage emplacement units are dominantly found in areas emplaced towards the end of the eruption. All investigated profiles for these locations were taken from the TDX dataset of 28/04/2015. Eruptive activity and inflation had ceased by this point (Pedersen et al., 2017) and thus the data represent an application of the investigated methods equivalent to planetary/palaeo-eruptive terrestrial scenarios.

5.2 Zones of Lava flow Inflation

Lava channel inflation occurred dominantly along the two central channels of the flow field, (Fig. 2B; see also figure 2 in Pedersen et al. (2017). Inflation of the southern channel was not captured well by the TDX data from 06/12/2014 due to artefacts generated by atmospheric heat propagating from the main crater Baugur westwards with the wind (see wave patterns in the central and eastern part of Fig. 2B). The magnitude and spatial extent of the inflation in the northern channel documented by the TDX data is in excellent agreement with high spatial and temporal resolution field observations reported in (Pedersen et al., 2017). Therefore, our investigation of the effect of channel inflation on the deduced rheological parameters focuses on

the northern channel (see profile locations in Fig. 2B and C). All investigated profiles were assessed for the change in the deduced rheological parameters between the 06/12/2014 and the 28/04/2015.

5.3 Pristine, Active Lava Flow Toes; Free of Inflation.

In order to calculate the morphology derived rheological parameters of actively flowing lava we identified locations where unconfined lava flow emplacement occurred during the time of DEM data acquisition (neither by levees nor a fully developed crust). These areas were identified by combining the available field data from the Icelandic Meteorological Office reports, MODIS satellite infrared images processed by MIROVA (Coppola et al., 2015) and Landsat satellite images (USGS). Due to changing eruption dynamics active lava toes were only covered by the TDX dataset from 06/12/2014, where breakouts occurred along the northern edge of the lava flow field. On 10/02/2015 activity was dominantly confined to inflation of the existing lava field and no active toes were captured by this TDX dataset. Therefore, all elevation profiles for the assessment of active flow toes were generated from the 06/12/2014 dataset.

The extreme heat of the active lava flow fronts (~1150℃; see Kolzenburg et al. (2017)) affects the TDX data. It causes variations in travel time of the radar waves depending on the vantage point of the two satellites and produces wave like patterns in the derived DEMs (see the zones east of the eruptive craters in Figure 2 B and D). This results in local zones of large scatter in the derived DEM data (Figure 3). This effect most likely results from the large density contrasts in the atmosphere above freshly exposed lava (i.e. between hot and cold air). Further, the temporal difference between the TerraSAR-X und TanDEM-X recordings were `10 sec during this recording phase, which could result in movement of these density contrast, inducing

the wave-pattern errors. We discard these data in our analyses and interpolate between the unaffected zones of the profiles.

We identified three (A1-3; Fig.2D) locations where longitudinal profiles of the active flow-front and four (A1-4; Fig 2D) locations where cross-sectional profiles of the active lava toes could be recovered. All cross sectional profile locations are set slightly upstream of the active flow front to avoid zones of large thermal scatter. Because flow was active during the time of TanDEM-X acquisition we assume that it was unconfined (with exception of the coolling induced rheologic contrast in the lava) at the flow front, where fresh lava was being emplaced continuously and the flow was in hydrostatic equilibrium. The identified profiles thus represent the geometry on the lava flow that is reflective of its rheological parameters during active flow advance.

6. Determination of Model Input Parameters

6.1 Density and Vesicularity

The density and vesicularity of the Holuhraun lava were determined via He-Pycnometry at the Department of Earth and Environmental Sciences, Ludwig-Maximilians-University of Munich. Measured density values range between 2700 and 2100 kg/m^3 for vesicularity ranging between 15 and 35 vol%. These values agree with the calculated, composition-dependent melt density of 2731 kg/m^3 for an eruptive temperature of 1100℃ using the model of Lange and Carmichael (1990). Therefore, the following calculations use an average value of 2050 kg/m^3 for lava density at 25 vol% vesicularity.

6.2 Effusion Rate

The time-dependent effusion rate of the Holuhraun eruption was reconstructed in great detail by Coppola et al. (2017), who combine measurements of radiative heat flux of the lava field measured using the MIROVA system (Coppola et al., 2016; D. Coppola 2013) with geometrical constraints on the magma storage region inside the Bárðarbunga caldera. Using these data, the effusion rate for 06/12/2014 could be constrained at ~100 m^3/sec.

The satellite derived values are in agreement with the geometry derived effusion rates calculated using the methods described in section 3. The calculated values, based on the range of individual flow dimensions reported in Pedersen et al. (2017), range between 70 and 128 m^3/sec for cooling limited flows of 11 to 16 km length, 800 to 1000 m width, 15 m height and a thermal diffusivity of the lava of 4 10^{-7} m^3s^{-1}. We, therefore, use 100 m^3/sec as a reasonable value for the volumetric effusion rate during the emplacement of the flow units investigated here.

6.3 Width, Height and Slope

Elevation profile locations were chosen as described in section 5. Lava flow width and height were determined by means of the TDX data for each profile location shown in Figure 2. Local and global slopes of the emplacement surface are very shallow and range from 0.2° to 0.5° with an average of 0.35°. These measurements were then combined with the average density, vesicularity, and effusive rate of the lava in order to calculate the rheological parameters following equations 4, 5, 6 and 7 for each profile.

7. Results

7.1 Standard Method

We measured the morphological parameters for 14 different profile locations in the lava flow-field that were emplaced as a single unit (Figure 4). The calculated rheological parameters are reported in Figure 5 and Table 1. The apparent viscosities range from $10^{4.3}$-$10^{5.4}$ Pa s for equation 4 and $10^{5.1}$-$10^{6.3}$ Pa s for equation 5. The calculated yield strengths range from $10^{2.8}$-$10^{3.1}$ Pa for equation 6 and $10^{2.9}$-$10^{3.5}$ Pa for equation 7. These data are in good agreement with the results from inflated sections of the lava flow (see Figures 6 and 7, described in the following chapter 7.2.), confirming that post-halting inflation, as observed in the field (Kolzenburg et al., 2017; Pedersen et al., 2017) was occurring even in flow lobes that were emplaced as a single unit.

7.2 Lava flow Inflation

Morphologically-derived rheologic parameters were calculated for 36 profile locations in five different sections of the lava flow field (34 samples for the TDX elevation difference between 06/12/2014 and 28/04/2015 and 2 samples for the difference between 10/02/2015 and 28/04/2015; Figure 6). The average calculated rheological parameters for each investigated section are reported with their respective standard errors in Figure 7 and individually in Table 2. Pre-inflation viscosities range from $10^{3.4}$-$10^{4.6}$ and $10^{4.5}$-$10^{5.3}$ for equations 4 and 5, respectively, and yield strengths range from $10^{2.6}$-$10^{2.8}$ Pa and $10^{3.7}$-$10^{2.3}$ Pa for equations 6 and 7, respectively. Inflation of the lava channels leads to a 1.0 – 5.2 m (18-200 %; with respect to the initial height) increase in average lava flow height without a significant change in flow width. This results in a 2.4 to 17 fold increase in the calculated apparent viscosity and 0.7 to 2.4 fold increase in the calculated yield strength. Final post emplacement values range from $10^{4.3}$-$10^{5.1}$ Pa

s and $10^{5.7}$-$10^{5.9}$ Pa s for equations 4 and 5, respectively and yield strengths range from $10^{2.9}$-$10^{3.9}$ Pa and $10^{3.2}$-$10^{3.7}$ Pa for equations 6 and 7, respectively. The data show a significant increase in the estimated viscosities between the 06/12/2014 and 28/04/2015 DEM datasets as a result of inflation. The increase in estimated viscosity due to inflation between 10/02/2015 and 28/04/2015 is smaller. The post-inflation data is in good agreement with the values recovered using the standard method, whereas pre-inflation data is significantly lower in all cases.

7.3 Active Flow Toes

The cross-sectional profiles of active sections at Holuhraun lava field are shown in Figure 8. The average calculated rheological parameters and respective standard errors for the active lava toes are plotted as red stars in Figure 7 and Table 3. Pre-inflation viscosities range from $10^{2.9}$-$10^{3.7}$ and $10^{3.8}$-$10^{4.9}$ for equations 4 and 5, respectively and yield strengths range from $10^{2.5}$-$10^{2.8}$ Pa and $10^{2.7}$-$10^{3.4}$ Pa for equations 6 and 7, respectively. The rheological parameters recovered for the active flow toes are the lowest measured values for equations 4, 5, and 6. However, they plot very close to the data measured for the confined lava channels, suggesting that on 06/12/2014 the lava inflation in the channel was minimal. The data calculated for equation 7 plots slightly above the values calculated for lava channel sections I1 and I2 at similar values to lava channel section I4. This is likely because the lava channel was confined by neighboring parts of the lava field, resulting in a reduced effective lava flow width that translates to a reduction in the calculated yield strengths, as width is in the divisor in this equation. Data recovered from the active lava toes are the lowest calculated values for equations 4, 5 and 6, whereas they represent an intermediate value for equation 7. This demonstrates that the application of the tested methods to post emplacement flow-geometries will in all cases result in an overestimation of the respective rheological parameters.

The difference between syn- and post-emplacement flow geometries is most obvious when comparing profiles of the lava flow fronts along the direction of flow emplacement. Figure 9 shows the longitudinal profiles of the flow front locations shown in Figure 2 A and D. Active toes are significantly lower and have much shallower flow front angles than post-emplacement flow fronts. This is the result of post-halting inflation, where the lava flow crust grew sufficiently strong to prevent further flow advance and the continued supply of viscous lava was accommodated by internal growth of the lava toe, resulting in vertical inflation and flow-front steepening.

8. Discussion

8.1 The Effect of Inflation on the Rheologic Parameters

Lava flows, both terrestrial and extra-terrestrial, display a large range in viscosities and shear strain rates and thus varying morphology (Cashman et al., 2013; Chevrel et al., 2014; Glaze and Baloga, 2006; Griffiths and Fink, 1992; Hiesinger et al., 2007; Hon et al., 2003; Hon et al., 1994; Keszthelyi et al., 2006; Nichols, 1939; Peterson and Tilling, 1980). At any given point in an inactive flow field the morphology is only recording the conditions of the lava after flow advance ceased. At the final stage of advance, sufficient surface crust is commonly formed to impede further flow front advancement, while the interior of the flow continues to be able to deform, resulting in inflation and hence a modified morphology (Hon et al., 1994; Kolzenburg et al., 2017; Walker, 1991).

For the 2014/15 Holuhraun lava flow field, the average apparent viscosities calculated for the post inflation lava are $10^{4.8}$ and $10^{5.7}$ Pa s for equations 4 and 5, respectively. The average yield strengths for the post inflation lava are $10^{2.9}$ and $10^{3.2}$ Pa for equations 6 and 7, respectively. These values are comparable to the values reported in Chevrel et al. (2013b) measured for lavas

of similar composition and volcanic setting. This demonstrates that the tested methods return reproducible results for comparable terrestrial settings. It further implies that inflation is an inherent problem in the determination of rheological parameters and that these previous estimates are most likely also affected by lava flow inflation and therefore represent an over estimate in both viscosity and yield strength. This is supported by the fact that viscosity values derived from the non-inflated, active emplacement stage (i.e. ones that correspond to the actual viscosity of the lava during flow) are lower than those estimated from flow morphology.

The data presented here show that the geometries of actively flowing lava (i.e. the stage of emplacement where rheologic parameters are applicable) in both confined and unconfined environments (i.e. single stage emplacement toes and active lava-channels) differ significantly from the post-emplacement geometries of inactive lava flows.

Inflation, which is commonplace in lava flows, results in an over-estimation of the lavas' rheological parameters of 0.8 and 1.1 log units in viscosity and 0.27 and 0.25 log units in yield strength for equations 4, 5, 6 and 7, respectively. This increase in calculated rheological parameters is higher for the dataset comparing the 06/12/2014 to the 28/04/2015 TDX data than for the dataset between 10/02/2015 and 28/04/2015. This difference is likely due to the decrease in effusion rate towards the end of the eruption and the resulting lower degree of inflation.

At a temperature of 1150℃ a 0.8 to 1.1 order of magnitude increase in viscosity implies a 14 to 19 wt% increase in silica content for the Holuhraun lava, (calculated using the viscosity model of Giordano et al. (2008)). Because of the decreasing fragility of melt viscosity with increasing silica content, this compositional uncertainty becomes more important with increasing silica content at common eruptive temperatures (1200-1050℃). This means that the correlation

of rheological parameters and composition is especially sensitive for high viscosity melts (i.e. high aspect ratio lava flows). That is an important issue consider when deducing compositional interpretations from morphological data on more evolved compositions as presented in Warner and Gregg (2003).

Although less critical than the errors in estimated viscosity, the estimation of apparent yield strength is also problematic. All common calculations are based on the assumption that no flow-impeding crust exists but that the morphology is a direct reflection of the lavas' internal forces. However, as outlined above, lava flow height is dominated by the strength of the developing rheological contrast zone (i.e. crust) that is governed by the balance between the rates of heat loss and lava-solidification. Thus, lava flow height is not correlated to the actual yield strength of the magmatic suspension in a rheological sense.

8.2 Implications for Interpreting Remote Sensing Data in Planetary Sciences

The presented data and analysis show that an increase in lava flow height due to inflation results in significant overestimation of all rheological parameters. The high viscosity values in the range of 10^5 to10^6 Pa s estimated from the morphology of Martian and Lunar lavas (Baloga et al., 2003; Glaze and Baloga, 2006; Hiesinger et al., 2007; Hulme and Fielder, 1977; Moore et al., 1978; Pasckert et al., 2012; Warner and Gregg, 2003; Wilson and Head, 1994; Zimbelman, 1985) for which compositional constraints would predict much lower viscosities (Chevrel et al., 2014; Musselwhite et al., 2006), could potentially be explained by high (>50 vol%) crystal contents (Chevrel et al., 2013b). However, suspensions with such high crystal contents are unlikely to achieve the long run-out distances documented by Martian lavas. Instead, widespread lava flow inflation, as documented for the Holuhraun example, is a much more likely reason for the observed mismatch between morphologically and compositionally inferred viscosities.

The lower calculated average apparent viscosities for active, non-inflated lava channels and individual toes (Fig. 7), representative of flowing lava prior to inflation, return more realistic values of $10^{3.8}$ to $10^{4.7}$ Pa s. This implies that lavas on other planets likely have lower effective flow viscosities than previously estimated.

Further, variations in environmental parameters such as surface- and eruptive-temperatures as well as the different precipitation, nature of the atmosphere and gravitational force on extra-terrestrial bodies may result in different emplacement dynamics. Griffiths and Fink (1992) and Keszthelyi et al. (2006) for example, show that the heat loss of lavas may vary widely between Earth, Mars and Venus and Moon/Io. Thus the efficiency of the development of an insulating and flow-impeding crust may vary drastically, which in turn influences the potential for lava flow inflation and the accompanying changes in lava flow aspect ratios. Colder surface temperatures, for example, favour crust formation, leading to earlier flow halting and consequently more intense inflation. Whereas higher surface temperatures retard crust formations resulting in lower degrees of inflation and thus flow geometries are more representative of the actual rheological parameters during emplacement. Further, the oxygen fugacity of the emplacement atmosphere can affect both the melt viscosity (Chevrel et al., 2013a; Di Genova et al., 2017) as well as its rheological solidification behaviour (Feig et al., 2010; Kolzenburg et al., 2018).

Therefore, accurate deduction of rheological parameters from morphological measurements needs to be benchmarked via environmental, morphological, petrological, and compositional constraints. The development and application of methods for accurate microanalysis of glass compositions in extra-terrestrial volcanic deposits, as presented in Di Genova et al. (2016), in conjunction with the rapidly growing availability of morphological data

on other planets e.g. (Baloga et al., 2003; Glaze and Baloga, 2006; Jaeger et al., 2007; Jaeger et al., 2010; James et al., 2015; Keszthelyi et al., 2008; Keszthelyi et al., 2006; Warner and Gregg, 2003; Williams et al., 2005; Wilson and Head, 1994) are crucial parts of furthering our understanding of the rheology of planetary volcanism.

8.3 Comparison to Laboratory Data

The lower calculated average apparent viscosities (10^4 to $10^{4.7}$ Pa s) for non-inflated lava flows (see Figure 7) is the closest value representative of flowing lava prior to inflation. These values reflect the lavas' viscosity at an emplacement-stage where lava flow advance ceased and further activity did not result in growth of the respective flow field section but rather its inflation. Therefore, they lend themselves for comparison with experimentally determined viscosities of crystallizing lavas.

The bulk cooling rate of the Holuhraun lava was reconstructed to lie between 0.2 and 0.8 K/min by Kolzenburg et al. (2017) The experimental results show that at a cooling rate of 0.5 K/min the viscosity of the Holuhraun lava starts to increase at around 1180℃ (at an absolute viscosity of around $10^{1.7}$ Pa s) and approaches its cut-off value (i.e. the point where the viscosity goes towards extreme values and flow ceases) at temperatures below 1120℃ (beyond an absolute viscosity of $10^{3.4}$Pa s). At lower oxygen fugacity, the T_{cutoff} values decrease, indicating the potential for longer runout distances under reduced conditions (Kolzenburg et al., 2018). This correlation between morphologically and experimentally determined lava flow stopping criteria suggests that the T_{cutoff} values measured in the laboratory accurately reproduce the morphologically derived viscosities at which lava flows stop and can, therefore, serve to improve existing computational lava flow models.

9. Conclusions

Based on the data presented in this study and the accompanying analysis and discussion, we draw the following conclusions:

1. Lava flow inflation results in a 2.4 to 17 fold overestimation of apparent viscosity and a 0.7 to 2.4 fold overestimation of yield strength for the methods commonly used in planetary science.
2. Previous estimates of rheological parameters on extra-terrestrial bodies may, at best, represent an upper limit, and actual viscosity values of these melts may be significantly lower.
3. The resulting uncertainty in the deduced lava compositions is large and increases for more evolved compositions.
4. Remote sensing and laboratory data are in reasonable agreement with respect to the absolute viscosity that determines the point at which lava flow advance ceases.
5. Bistatic SAR Missions and the derived height information prove to be a valuable tool for monitoring lava flow fields. Future SAR missions with this capability would be very important for research in remote sensing.

Acknowledgements

We would like to thank Daniele Giordano, Department of Earth Sciences, University of Turin, for interesting discussions on lava rheology along the way and Kai Uwe Hess, Department of Earth and Environmental Sciences, Section Mineralogy, Ludwig-Maximilians-University Munich, for discussions on the Holuhraun eruption and connecting our research groups. The remote sensing data used in this study was made available within the 3 year project IsViews

(Iceland subglacial Volcanoes interdisciplinary early warning system), where funding by the Bavarian Ministry of Economic Affairs and Media, Energy and Technology (ID 20-8-3410.2-15-2012) and the Bavarian State Ministry of Sciences, Research and the Arts (Kz 1507 12032) is gratefully acknowledged. The German Aerospace Centre (DLR), Remote Sensing Technology Institute is gratefully acknowledged for providing and pre-processing TerraSAR-X and TanDEM-X data within the IsViews project (TDX-CoSSC Science Proposal OTHER 2375, PI: C. Minet); Special thanks goes to Thomas Fritz, Christian Minet and Michael Eineder for discussions on the technical details of the TanDEM-X data. The German company GeoFly is acknowledged for acquiring and processing the airborne UltraCam data within the project IsViews. We also thank Planet Labs Germany for supplying the RapidEye data of Iceland in the framework of DLR/RESA proposal ID 619. Àgúst Guðmundsson, Fjarkönnun ehf., is grateful acknowledged for his support with the organisation of the field work, especially the flight management in Iceland with the UltraCam Xp camera. The IsViews team also thanks the Icelandic research centre (Rannsóknamiðstöð Islands) and the director of the Vatnajökull National Park, Þórður H Ólafsson for granting fieldwork permits (2/2014; 13/2015; 12/2016 and 4/2017). D. B. Dingwell acknowledges the support of ERC Advanced Grant 247076 "EVOKES".

10. References

Baloga, S.M., Glaze, L.S., Peitersen, M.N. and Crisp, J.A., 2001. Influence of volatile loss on thickness and density profiles of active basaltic flow lobes. Journal of Geophysical Research: Solid Earth, 106(B7): 13395-13405.

Baloga, S.M., Mouginis-Mark, P.J. and Glaze, L.S., 2003. Rheology of a long lava flow at Pavonis Mons, Mars. Journal of Geophysical Research: Planets, 108(E7): n/a-n/a.

Bruno, B.C., Taylor, G.J., Rowland, S.K. and Baloga, S.M., 1994. Quantifying the effect of rheology on lava-flow margins using fractal geometry. Bulletin of Volcanology, 56(3): 193-206.

Cashman, K., Soule, S., Mackey, B., Deligne, N., Deardorff, N. and Dietterich, H., 2013. How lava flows: New insights from applications of lidar technologies to lava flow studies. Geosphere, 9(6): 1664-1680.

Cashman, K.V., Thornber, C. and Kauahikaua, J.P., 1999. Cooling and crystallization of lava in open channels, and the transition of Pāhoehoe Lava to 'A'ā. Bulletin of Volcanology, 61(5): 306-323.

Chevrel, M.O., Baratoux, D., Hess, K.-U. and Dingwell, D.B., 2014. Viscous flow behavior of tholeiitic and alkaline Fe-rich martian basalts. Geochimica et Cosmochimica Acta, 124(0): 348-365.

Chevrel, M.O., Giordano, D., Potuzak, M., Courtial, P. and Dingwell, D.B., 2013a. Physical properties of $CaAl_2Si_2O_8$–$CaMgSi_2O_6$–FeO–Fe_2O_3 melts: Analogues for extra-terrestrial basalt. Chemical Geology, 346: 93-105.

Chevrel, M.O., Platz, T., Hauber, E., Baratoux, D., Lavallée, Y. and Dingwell, D.B., 2013b. Lava flow rheology: A comparison of morphological and petrological methods. Earth Planet. Sci. Lett., 384(0): 109-120.

Coppola, D., Laiolo, M., Cigolini, C., Delle Donne, D. and Ripepe, M., 2015. Enhanced volcanic hot-spot detection using MODIS IR data: results from the MIROVA system. Geological Society, London, Special Publications, 426: SP426. 425.

Coppola, D., Laiolo, M., Cigolini, C., Delle Donne, D. and Ripepe, M., 2016. Enhanced volcanic hot-spot detection using MODIS IR data: results from the MIROVA system. Geological Society, London, Special Publications, 426(1): 181-205.

Coppola, D., Ripepe, M., Laiolo, M. and Cigolini, C., 2017. Modelling satellite-derived magma discharge to explain caldera collapse. Geology: G38866. 38861.

D. Coppola , M.L., D. Piscopo, C. Cigolini, 2013. Rheological control on the radiant density of active lava flows and domes.

Decker, R.W., Wright, T.L. and Stauffer, P.H., 1987. Volcanism in Hawaii. US Government Printing Office.

Di Genova, D., Kolzenburg, S., Vona, A., Chevrel, M.O., Hess, K.-U., Neuville, D.R., Ertel-Ingrisch, W., Romano, C. and Dingwell, D.B., 2016. Raman spectra of Martian glass analogues: A tool to approximate their chemical composition. Journal of Geophysical Research: Planets: n/a-n/a.

Di Genova, D., Vasseur, J., Hess, K.-U., Neuville, D.R. and Dingwell, D.B., 2017. Effect of oxygen fugacity on the glass transition, viscosity and structure of silica-and iron-rich magmatic melts. Journal of Non-Crystalline Solids, 470: 78-85.

Dirscherl, M. and Rossi, C., 2018. Geomorphometric analysis of the 2014–2015 Bárðarbunga volcanic eruption, Iceland. Remote Sensing of Environment, 204: 244-259.

Farquharson, J., James, M. and Tuffen, H., 2015. Examining rhyolite lava flow dynamics through photo-based 3D reconstructions of the 2011–2012 lava flowfield at Cordón-Caulle, Chile. Journal of Volcanology and Geothermal Research, 304: 336-348.

Favalli, M., Fornaciai, A., Mazzarini, F., Harris, A., Neri, M., Behncke, B., Pareschi, M.T., Tarquini, S. and Boschi, E., 2010. Evolution of an active lava flow field using a multitemporal LIDAR acquisition. Journal of Geophysical Research: Solid Earth (1978–2012), 115(B11).

Feig, S.T., Koepke, J. and Snow, J.E., 2010. Effect of oxygen fugacity and water on phase equilibria of a hydrous tholeiitic basalt. Contributions to Mineralogy and Petrology, 160(4): 551-568.

Fink, J.H. and Griffiths, R.W., 1990. Radial spreading of viscous-gravity currents with solidifying crust. Journal of Fluid Mechanics, 221: 485-509.

Giordano, D., Polacci, M., Longo, A., Papale, P., Dingwell, D., Boschi, E. and Kasereka, M., 2007. Thermo-rheological magma control on the impact of highly fluid lava flows at Mt. Nyiragongo. Geophys. Res. Lett., 34(6).

Giordano, D., Russell, J.K. and Dingwell, D.B., 2008. Viscosity of magmatic liquids: A model. Earth Planet. Sci. Lett., 271(1–4): 123-134.

Gíslason, S., Stefánsdóttir, G., Pfeffer, M., Barsotti, S., Jóhannsson, T., Galeczka, I., Bali, E., Sigmarsson, O., Stefánsson, A. and Keller, N., 2015. Environmental pressure from the 2014–15 eruption of Bárðarbunga volcano, Iceland. Geochem. Perspect. Lett, 1: 84-93.

Glaze, L.S. and Baloga, S.M., 2006. Rheologic inferences from the levees of lava flows on Mars. Journal of Geophysical Research: Planets, 111(E9): n/a-n/a.

Glaze, L.S., Baloga, S.M. and Stofan, E.R., 2003. A methodology for constraining lava flow rheologies with MOLA. Icarus, 165(1): 26-33.

Gregg, T.K. and Fink, J.H., 2000. A laboratory investigation into the effects of slope on lava flow morphology. J. Volcanol. Geotherm. Res., 96(3): 145-159.

Griffiths, R.W. and Fink, J.H., 1992. The morphology of lava flows in planetary environments: Predictions from analog experiments. Journal of Geophysical Research.

Gruber, M., Ponticellia, M., Bernögger, S. and Leberl, L., 2008. UltraCamX, the large format digital aerial camera system by Vexcel Imaging/Microsoft, Proceedings of ISPRS XXIst Congress "Silk Road for Information from Imagery, pp. 3-11.

Hajnsek, I. and Busche, T., 2015. TanDEM-X: science activities, Geoscience and Remote Sensing Symposium (IGARSS), 2015 IEEE International. IEEE, pp. 2892-2894.

Hiesinger, H., Head, J. and Neukum, G., 2007. Young lava flows on the eastern flank of Ascraeus Mons: Rheological properties derived from High Resolution Stereo Camera (HRSC) images and Mars Orbiter Laser Altimeter (MOLA) data. Journal of Geophysical Research: Planets, 112(E5).

Hon, K., Gansecki, C. and Kauahikaua, J., 2003. The Transition from'A'a to Pahoehoe Crust on Flows Emplaced During the Pu'u'6'6-Kupaianaha Eruption. US Geological Survey professional paper, 1676: 89.

Hon, K., Kauahikaua, J., Denlinger, R. and Mackay, K., 1994. Emplacement and inflation of pahoehoe sheet flows: Observations and measurements of active lava flows on Kilauea Volcano, Hawaii. Geological Society of America Bulletin, 106(3): 351-370.

Hulme, G., 1974. The Interpretation of Lava Flow Morphology. Geophysical Journal International, 39(2): 361-383.

Hulme, G. and Fielder, G., 1977. Effusion rates and rheology of lunar lavas. Philosophical Transactions of the Royal Society of London A: Mathematical, Physical and Engineering Sciences, 285(1327): 227-234.

Jaeger, W., Keszthelyi, L., McEwen, A., Dundas, C. and Russell, P.S., 2007. Athabasca Valles, Mars: A lava-draped channel system. Science, 317(5845): 1709-1711.

Jaeger, W., Keszthelyi, L., Skinner, J., Milazzo, M., McEwen, A., Titus, T., Rosiek, M., Galuszka, D., Howington-Kraus, E. and Kirk, R., 2010. Emplacement of the youngest flood lava on Mars: A short, turbulent story. Icarus, 205(1): 230-243.

Jaenicke, J., Münzer, U., Mayer, C., Minet, C., Franke, J., Siegert, F. and Guðmundsson, Á., 2014. Überwachung isländischer Vulkane mit innovativen Fernerkundungs-Technologien und 3D Visualisierung. Fernerkundungs-Technologien und 3D Visualisierung. 34. Wissenschaftlich-Technische Jahrestagung der DGPF(Geoinformationen Öffnen das Tor zur Welt): 1-14.

Jaenicke, J., Münzer, U., Minet, C., Eineder, M., Braun, L., Siegert, F. and Gudmundsson, A., 2016. Volcanic activity at Bárðarbunga, Iceland, monitored with TerraSAR-X and TanDEM-X data. TerraSAR-X/ TanDEM-X Science Team Meeting Oberpfaffenhofen, Germany, 17-20 October 2016.

James, P.B., Zuber, M.T., Phillips, R.J. and Solomon, S.C., 2015. Support of long-wavelength topography on Mercury inferred from MESSENGER measurements of gravity and topography. Journal of Geophysical Research: Planets, 120(2): 287-310.

Keszthelyi, L., Jaeger, W., McEwen, A., Tornabene, L., Beyer, R.A., Dundas, C. and Milazzo, M., 2008. High Resolution Imaging Science Experiment (HiRISE) images of volcanic terrains from the first 6 months of the Mars Reconnaissance Orbiter primary science phase. Journal of Geophysical Research: Planets, 113(E4).

Keszthelyi, L., Self, S. and Thordarson, T., 2006. Flood lavas on earth, Io and Mars. Journal of the geological society, 163(2): 253-264.

Kolzenburg, S., Di Genova, D., Giordano, D., Hess, K.U. and Dingwell, D.B., 2018. The effect of oxygen fugacity on the rheological evolution of crystallizing basaltic melts. Earth and Planetary Science Letters, 487: 21-32.

Kolzenburg, S., Favalli, M., Fornaciai, A., Isola, I., Harris, A.J.L., Nannipieri, L. and Giordano, D., 2016a. Rapid Updating and Improvement of Airborne LIDAR DEMs Through Ground-Based SfM 3-D Modeling of Volcanic Features. IEEE Transactions on Geoscience and Remote Sensing, PP(99): 1-13.

Kolzenburg, S., Giordano, D., Cimarelli, C. and Dingwell, D.B., 2016b. In Situ thermal characterization of cooling/crystallizing lavas during rheology measurements and implications for lava flow emplacement. Geochimica et Cosmochimica Acta(195): 244-258.

Kolzenburg, S., Giordano, D., Thordarson, T., Höskuldsson, A. and Dingwell, D.B., 2017. The rheological evolution of the 2014/2015 eruption at Holuhraun, central Iceland. Bulletin of Volcanology, 79(6): 45.

Krieger, G., Moreira, A., Fiedler, H., Hajnsek, I., Werner, M., Younis, M. and Zink, M., 2007. TanDEM-X: A satellite formation for high-resolution SAR interferometry. IEEE Transactions on Geoscience and Remote Sensing, 45(11): 3317-3341.

Lange, R. and Carmichael, I.S., 1990. Thermodynamic properties of silicate liquids with emphasis on density, thermal expansion and compressibility. Reviews in Mineralogy and Geochemistry, 24(1): 25-64.

Mayer, C., Jaenicke, J., Lambrecht, A., Braun, L., Völksen, C., Minet, C. and Münzer, U., 2016. Local surface mass-balance reconstruction from a tephra layer–a case study on the northern slope of Mýrdalsjökull, Iceland. Journal of Glaciology, 63(237): 79-87.

Moore, H., Arthur, D. and Schaber, G., 1978. Yield strengths of flows on the Earth, Mars, and Moon, Lunar and planetary science conference proceedings, pp. 3351-3378.

Münzer, U., Jaenicke, J., Eineder, M., Minet, C., Braun, L., Mayer, C., Siegert, F. and Franke, J., 2016. Anwendung neuer Methoden mit hochauflösenden Fernerkundungs-daten (TerraSAR-X, TanDEM-X, RapidEye, UltraCam, HRSC) zur Früherkennung subglazialer Vulkanausbrüche auf Island, final report, 1-85.

Münzer, U., Mayer, C., Reichel, L., Runge, H., Fritz, T., Rossi, C. and Gudmundsson, À., 2010. NRT-monitoring am Vulkanausbruch Eyjafjallajökull (Island) mit TerraSAR-X. Photogrammetrie-Fernerkundung-Geoinformation PFG(5): 339-354.

Musselwhite, D.S., Dalton, H.A., Kiefer, W.S. and Treiman, A.H., 2006. Experimental petrology of the basaltic shergottite Yamato-980459: Implications for the thermal structure of the Martian mantle. Meteoritics & Planetary Science Archives, 41(9): 1271-1290.

Nichols, R.L., 1939. Viscosity of lava. The Journal of Geology, 47(3): 290-302.

Orowan, E., 1949. Remarks at joint meeting of the British Glaciological Society, the British Rheologists Club and the Institute of Metals. J. Glaciol, 1: 231-236.

Pasckert, J.H., Hiesinger, H. and Reiss, D., 2012. Rheologies and ages of lava flows on Elysium Mons, Mars. Icarus, 219(1): 443-457.

Pedersen, G.B.M., Höskuldsson, A., Dürig, T., Thordarson, T., Jónsdóttir, I., Riishuus, M.S., Óskarsson, B.V., Dumont, S., Magnusson, E., Gudmundsson, M.T., Sigmundsson, F., Drouin, V.J.P.B., Gallagher, C., Askew, R., Guðnason, J., Moreland, W.M., Nikkola, P., Reynolds, H.I. and Schmith, J., 2017. Lava field evolution and emplacement dynamics of the 2014–2015 basaltic fissure eruption at Holuhraun, Iceland. Journal of Volcanology and Geothermal Research.

Peterson, D.W. and Tilling, R.I., 1980. Transition of basaltic lava from pahoehoe to aa, Kilauea Volcano, Hawaii: Field observations and key factors. J. Volcanol. Geotherm. Res., 7(3–4): 271-293.

Pinkerton, H. and Wilson, L., 1994. Factors controlling the lengths of channel-fed lava flows. Bulletin of Volcanology, 56(2): 108-120.

Rossi, C., Gonzalez, F.R., Fritz, T., Yague-Martinez, N. and Eineder, M., 2012. TanDEM-X calibrated raw DEM generation. ISPRS Journal of Photogrammetry and Remote Sensing, 73: 12-20.

Rossi, C., Minet, C., Fritz, T., Eineder, M. and Bamler, R., 2016. Temporal monitoring of subglacial volcanoes with TanDEM-X—Application to the 2014–2015 eruption within the Bárðarbunga volcanic system, Iceland. Remote Sensing of Environment, 181: 186-197.

Ruch, J., Wang, T., Xu, W., Hensch, M. and Jónsson, S., 2016. Oblique rift opening revealed by reoccurring magma injection in central Iceland. Nature communications: 1-7.

Sigmundsson, F., Hooper, A., Hreinsdóttir, S., Vogfjörd, K.S., Ófeigsson, B.G., Heimisson, E.R., Dumont, S., Parks, M., Spaans, K. and Gudmundsson, G.B., 2014. Segmented lateral dyke growth in a rifting event at Barðarbunga volcanic system, Iceland. Nature, 517(08 January 2015): 191-195.

Walker, G., 1991. Structure, and origin by injection of lava under surface crust, of tumuli, “lava rises”, “lava-rise pits”, and “lava-inflation clefts” in Hawaii. Bulletin of Volcanology, 53(7): 546-558.

Warner, N.H. and Gregg, T.K., 2003. Evolved lavas on Mars? Observations from southwest Arsia Mons and Sabancaya volcano, Peru. Journal of Geophysical Research: Planets, 108(E10).

Wiechert, A., Gruber, M. and Ponticelli, M., 2011. UltraCam: the new superlarge format digital aerial camera, Proc. of the ASPRS 2011 Annual Conference, Milwaukee, Wisconsin.

Williams, D.A., Keszthelyi, L.P., Schenk, P.M., Milazzo, M.P., Lopes, R.M., Rathbun, J.A. and Greeley, R., 2005. The Zamama–Thor region of Io: Insights from a synthesis of mapping, topography, and Galileo spacecraft data. Icarus, 177(1): 69-88.

Wilson, L. and Head, J.W., 1994. Mars: Review and analysis of volcanic eruption theory and relationships to observed landforms. Reviews of Geophysics, 32(3): 221-263.

Zimbelman, J.R., 1985. Estimates of rheologic properties for flows on the Martian volcano Ascraeus Mons. Journal of Geophysical Research: Solid Earth, 90(S01): 157-162.

11. Figure Captions

Figure 1: Overview of Eruption Site

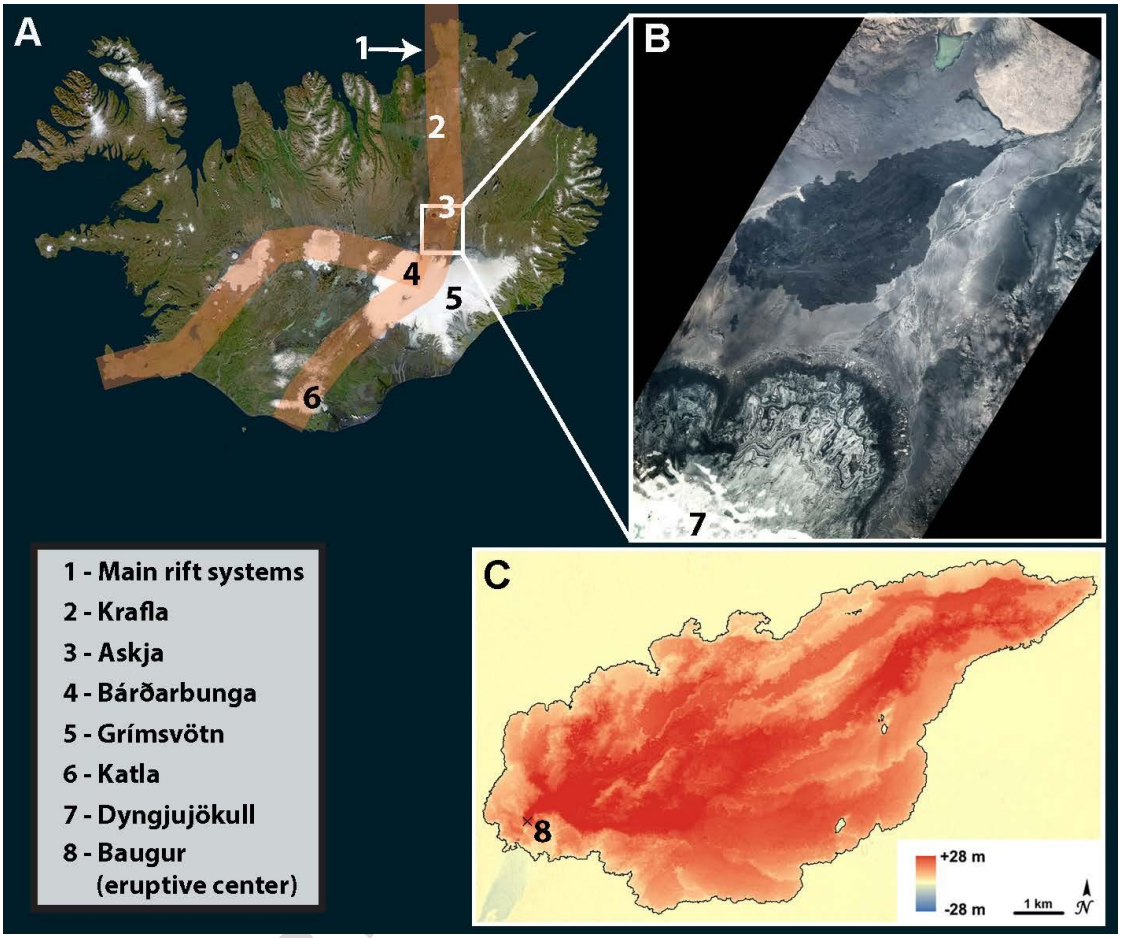

Figure 1: A) RapidEye satellite mosaic of Iceland with the Neovolcanic Zone (1) and some iconic volcanic centres (2-6) within the rift system. The Holuhraun eruption site is located in the white square between the subglacial central volcano Bárðarbunga and the Askja caldera (RapidEye mosaic, Planet Labs Germany, DLR/RESA proposal ID 619, compiled by RSS GmbH within the project IsViews) B) Enlargement of the square in (A) showing an UltraCam mosaic from 08/09/2015; 20 cm pixel resolution, covering the final extent of the Holuhraun lava field (85 km^2) located south of Askja caldera and north of the outlet glacier Dyngjujökull © IsViews. C) TanDEM-X difference, calculated between 22/01/2011 and 28/04/2015, showing various lava flow channels within the lava field [raw data © DLR]. The eruptive centre, called Baugur crater (8), is located in the south west of the lava field.

Figure 2: Profile Locations

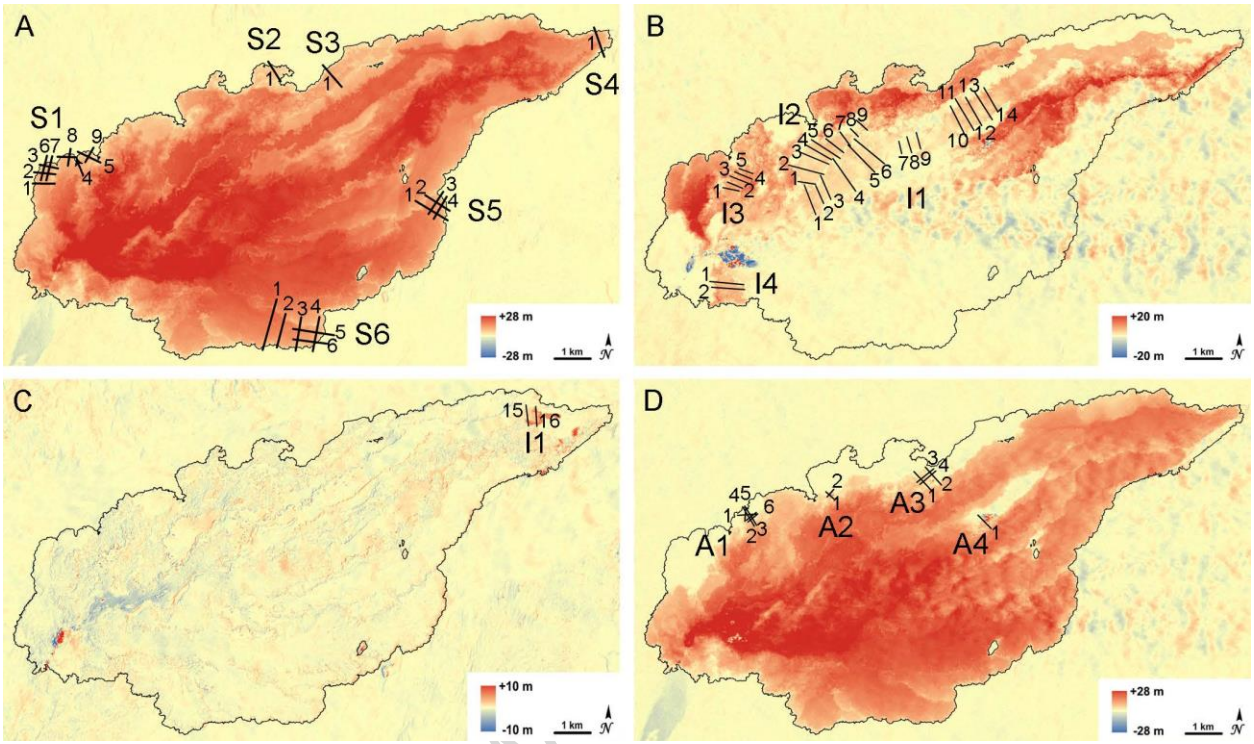

Figure 2: Overview over the individual profile locations identified by means of TanDEM-X difference. A) DEM difference between 28/04/2015 and 22/01/2011 showing the absolute elevation difference between pre and post eruption surfaces. This image was used to identify locations for the standard approach of deducing rheology from morphology of single flow units. Six zones (S1-6) were selected to recover a total of 22 cross sectional and longitudinal post eruption profiles. B) DEM difference between 28/04/2015 and 06/12/2014 showing areas of lava flow inflation. This image was used to identify locations in which inflation had occurred in previously existing lava channels. Four zones (I1-4) were selected to recover a total of 34 cross sectional profiles from both the 28/04/2015 and 06/12/2014 TDX datasets. C) DEM difference between 28/04/2015 and 15/02/2015 showing areas of lava flow inflation between 10/02/2015 and the end of the eruption. Two additional cross sectional profiles of Zone I1 were selected from this dataset to assess the degree of inflation between 15/02/2015.and 28/04/2015 D) DEM difference between 06/12/2014 and 15/02/2015. Four zones (A1-4) were selected to recover a total of 12 cross sectional and longitudinal post eruption profile from the 06/12/2014 TDX dataset. This image was also used to identify zones of localized thermal instabilities in areas of active lava flow emplacement.

Figure 3: Thermally Induced Scatter in Radar Data

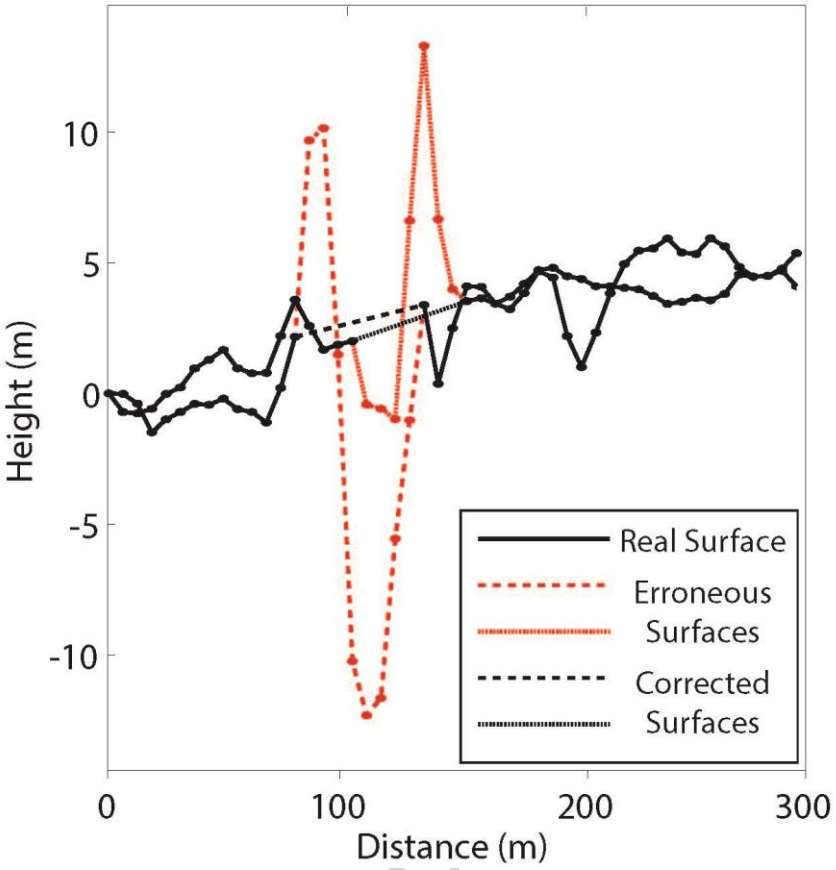

Figure 3: Examples of the thermally induced scatter in the TDX data from 06/12/2014 at active lava flow fronts. Areas of high thermal activity produce up to > ±10 m scatter in the DEM recovered from the radar data (red dotted and dashed lines). Solidified lava flow surfaces are not affected by this scatter (solid black lines). Where present, these gaps were interpolated (black dotted and dashed lines).

Figure 4: Elevation Profiles for Standard Approach

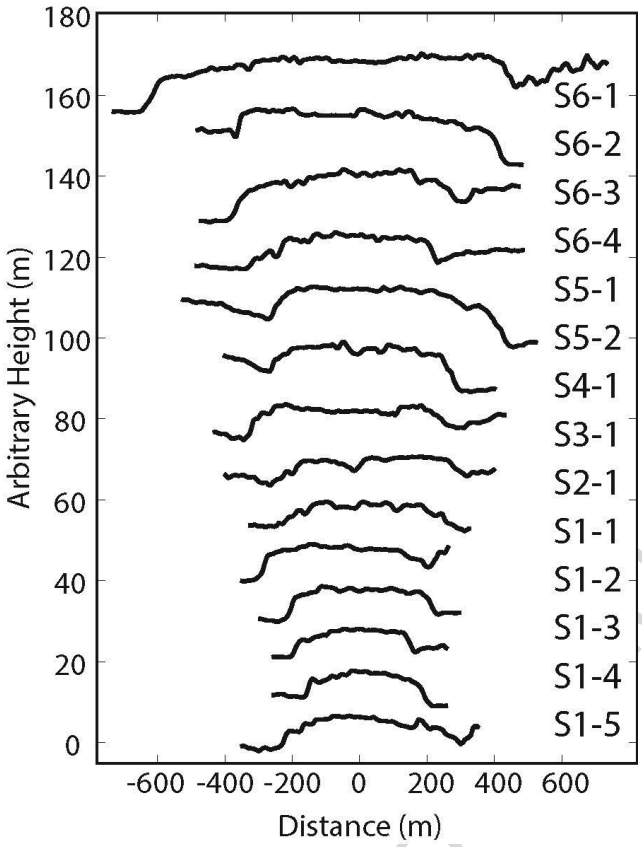

Figure 4: Plot of 14 elevation profiles generated from the TDX DEM of the 28/04/2015. The profiles are used to recover rheological parameters of lava flow lobes emplaced as a single unit. Profile locations are shown in Figure 2. Although the width varies significantly, the calculated rheological parameters return similar values (see Fig. 5).

Figure 5: Calculated Results from Standard Approach

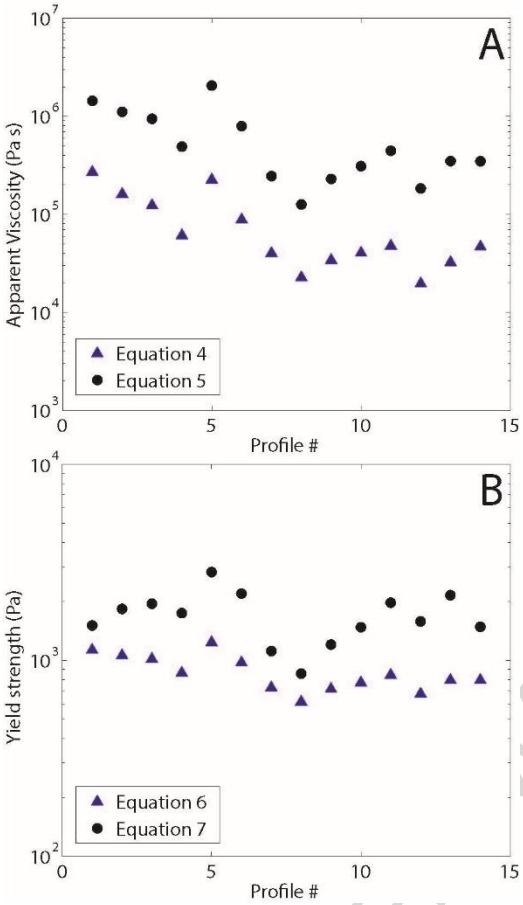

Figure 5: Rheological parameters calculated for the profiles of lava flow lobes emplaced as a single unit. A) Viscosities calculated with Equations 4 and 5 are plotted as black dots and blue triangles, respectively. Data returned by equation 5 are consistently higher than those for equation 4. B) Yield strengths calculated with equations 6 and 7 are plotted as black dots and blue triangles, respectively. Values returned by equation 7 are consistently higher than those for equation 6. Despite some scatter, the overall order of magnitude returned for all profile locations falls within a narrow range, indicating a good consistency for all four methods.

Figure 6: Elevation Profiles for Inflated Sections

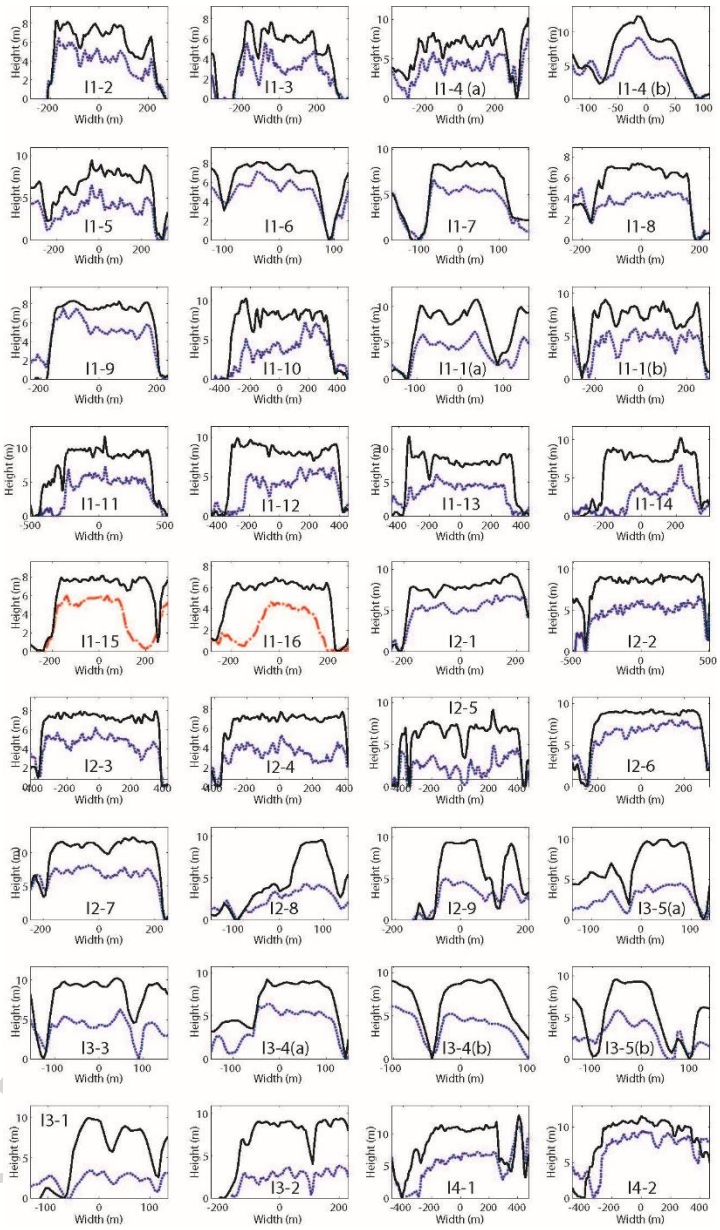

Figure 6: Summary plot of the inflation profiles investigated for this study. Profiles from the DEM of TanDEM-X data from 06/12/2014 are plotted as dotted, blue lines. Profiles from 28/04/2015 are plotted in solid black. Two profiles where inflation occurred between 10/02/2015 and 28/04/2015 are plotted as dashed, red lines. Profiles are labelled according to figure 2. Profiles labelled with small letters (a) or (b) correspond to sub-sections of the respective profile locations in figure 2 where the profile lines spans more than one individual flow. Inflation is in most cases restricted to vertical growth of the lava flows with little to no horizontal expansion. Horizontal growth is only detected in the two examples of inflation between the February and April datasets.

Figure 7: Calculated Results from Inflated Sections

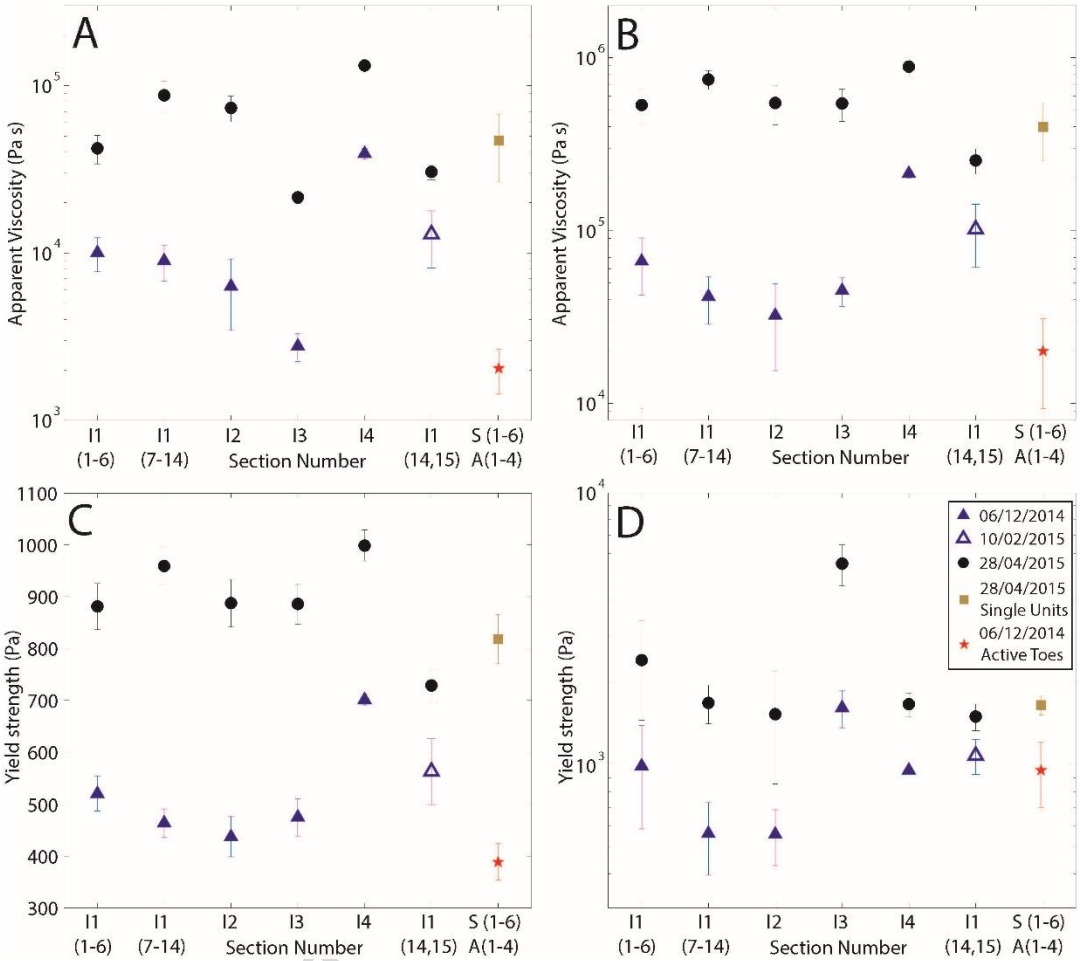

Figure 7: Results from the investigations of inflation of the Holuhraun lava flow field. Viscosities calculated with equations 4 and 5 are plotted in sub-plots A and B, respectively. Yield strengths calculated with equations 6 and 7 are plotted in sub-plots C and D, respectively. Data are reported as averages of all profiles in each section together with the respective standard error. Pre-inflation data are plotted as blue filled and open triangles for the 06/12/2014 and 10/02/2015 datasets, respectively; Post-inflation data from 28/04/2015 are plotted as black dots. Average and standard error for the standard approach data shown in figure 4 are plotted as a brown square. Average and standard error for the active lava toes are plotted as a red star.

Figure 8: Elevation Profiles of Active Lava Flows

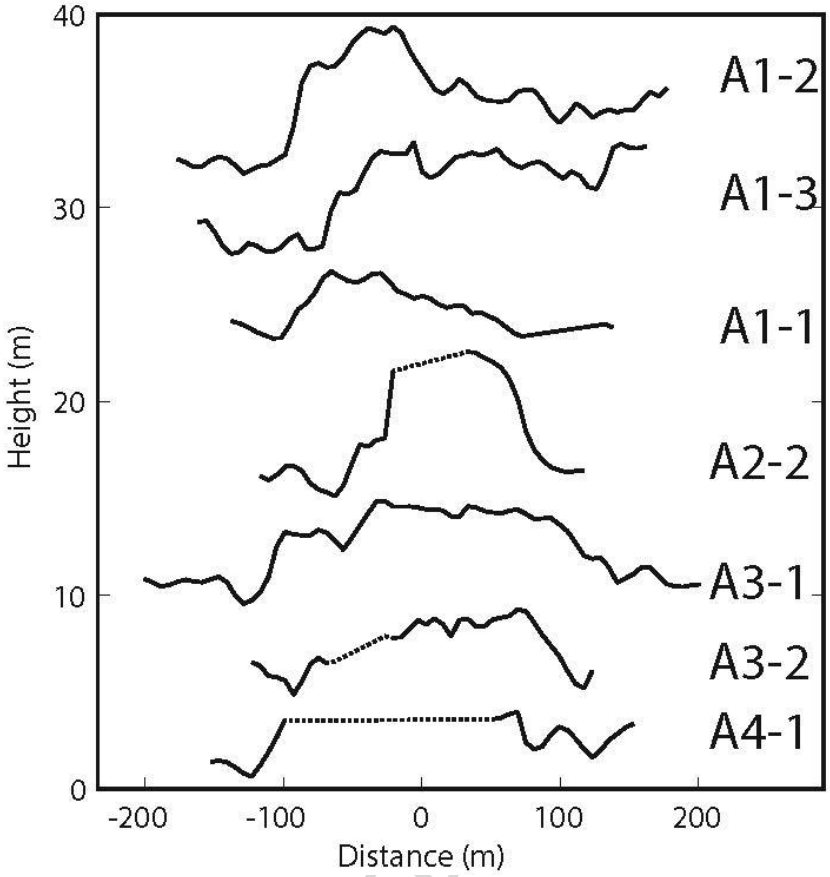

Figure 8: Summary plot of all profiles used to recover rheological parameters of active lava flow toes. Profile locations are shown in Figure 2. Areas where the TDX elevation data (06/12/2014) were affected by thermally induced scatter (see Figure 3) were interpolated and are shown as dotted lines.

Figure 9: Inflation of Lava Flow Fronts

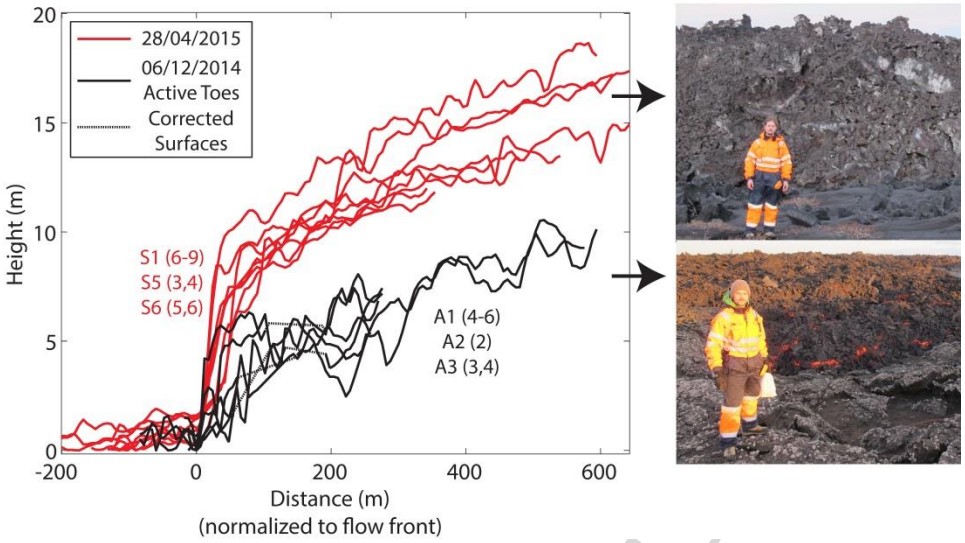

Figure 9: Summary plot of all profiles of lava flow fronts shown in Figure 2. There is a drastic difference in both front-angle (~40 vs. ~80 degrees) and –height (~5 vs. ~10) between active and post-emplacement, inflated flow fronts. Areas where the TanDEM-X data were affected by the thermal scatter (see Figure 3) were interpolated and are shown as dotted lines. Photographs on the right show examples of active and inflated lava flow-field sections with a person for scale. Photos were taken on the SW flow field on the 20/11/2014; ©S. Kolzenburg.

12. Tables

Table 1: Morphology derived rheological parameters for Profiles in figure 2A. Values are calculated after equations 4,5,6 and 7 for η2, η3, τ1 and τ2, respectively

Profile	*w (m)*	*h (m)*	*Log 10 (η2)* *Pa s*	*Log 10 (η3)* *Pa s*	*Log 10 (τ1)* *Pa*	*Log 10 (τ2)* *Pa*
S1-1	534	6.3	5.4	6.2	2.9	3.2
S1-2	480	6.9	5.2	6.0	2.9	3.3
S1-3	384	5.5	5.1	6.0	2.8	3.2
S1-4	390	6.5	4.8	5.7	2.9	3.3
S1-5	564	6.5	5.4	6.3	2.9	3.2
S2-1	564	5.8	4.9	5.9	2.9	3.1
S3-1	588	5.0	4.6	5.4	2.8	2.9
S4-1	630	5.9	4.4	5.1	2.9	3.0
S5-1	720	10.1	4.5	5.4	3.1	3.5
S5-2	576	7.9	4.6	5.5	3.0	3.3
S6-1	1128	9.2	4.7	5.6	3.1	3.2
S6-2	816	8.6	4.3	5.3	3.0	3.3
S6-3	708	8.3	4.5	5.5	3.0	3.3
S6-4	570	7.0	4.7	5.5	2.9	3.2

Table 2: Morphology derived rheological parameters for profiles in figure 2A. Values are calculated after equations 4,5,6 and 7 for η2, η3, τ1 and τ2, respectively. Values are repoprted for the 06/12/2014 and the 28/04/2015 with exception of I1-15 and I1-16, where the data are reported for the 10/02/2015 and the 28/04/2015; see figure 2 for profile locations and figure 6 for profile shapes

Profile	*w (m) 12/2014*	*w (m) 02/2015*	*h (m) 12/2014*	*h (m) 02/2015*	*Log 10 (η2) (Pa s) 12/2014*	*Log 10 (η2) (Pa s) 02/2015*	*Log 10 (η3) (Pa s) 12/2014*	*Log 10 (η3) (Pa s) 02/2015*	*Log 10 (τ1) (Pa) 12/2014*	*Log 10 (τ1) (Pa) 02/2015*	*Log 10 (τ2) (Pa) 12/2014*	*Log 10 (τ2) (Pa) 02/2015*
I1-1(a)	198	210	3.7	8.2	3.5	4.5	4.6	6.0	2.7	3.0	3.1	3.8
I1-1(b)	516	552	4.5	7.2	4.2	4.8	4.9	5.7	2.7	2.9	2.9	3.3
I1-2	492	492	5.4	8.5	4.4	5.0	5.2	6.0	2.8	3.0	3.1	3.5
I1-3	582	588	4.5	7.1	4.2	4.8	4.9	5.7	2.7	2.9	2.8	3.2
I1-4(a)	630	624	3.8	6.0	4.0	4.6	4.6	5.4	2.7	2.9	2.7	3.1
I1-4(b)	162	162	5.8	8.8	4.0	4.5	5.4	6.1	2.9	3.0	3.6	4.0
I1-5	510	516	3.6	6.5	3.8	4.6	4.5	5.6	2.6	2.9	2.7	3.2
I1-6	186	192	4.0	6.1	3.6	4.1	4.7	5.4	2.7	2.9	3.2	3.6
I1-7	234	258	4.6	7.0	3.8	4.4	4.9	5.7	2.7	2.9	3.3	3.6
I1-8	354	372	3.3	5.9	3.6	4.4	4.4	5.4	2.6	2.9	2.8	3.3
I1-9	402	396	5.0	7.7	4.2	4.7	5.1	5.9	2.8	3.0	3.1	3.5
I1-10	678	756	3.6	8.0	4.0	5.1	4.5	5.9	2.6	3.0	2.6	3.2
I1-11	750	894	4.7	8.7	4.4	5.3	5.0	6.1	2.8	3.0	2.8	3.2
I1-12	672	780	4.0	7.9	4.1	5.1	4.7	5.9	2.7	3.0	2.7	3.2
I1-13	696	786	3.4	8.0	3.9	5.1	4.4	5.9	2.6	3.0	2.5	3.2
I1-14	432	576	3.4	6.9	3.7	4.8	4.4	5.7	2.6	2.9	2.7	3.2
I1-15	432	456	5.3	6.3	4.3	4.5	5.2	5.5	2.8	2.9	3.1	3.2
I1-16	348	492	3.9	5.6	3.8	4.4	4.6	5.3	2.7	2.8	2.9	3.1
I2-1	456	456	3.6	5.9	3.8	4.5	4.5	5.4	2.6	2.9	2.7	3.2
I2-2	882	906	4.3	8.1	4.3	5.2	4.8	5.9	2.7	3.0	2.6	3.2
I2-3	780	774	4.2	7.0	4.2	4.9	4.8	5.7	2.7	2.9	2.7	3.1
I2-4	798	780	2.7	5.8	3.7	4.7	4.0	5.4	2.5	2.9	2.3	2.9
I2-5	804	798	2.5	7.1	3.6	4.9	3.9	5.7	2.5	2.9	2.2	3.1
I2-6	552	552	5.3	7.6	4.4	4.9	5.2	5.8	2.8	3.0	3.0	3.3
I2-7	438	432	4.9	9.4	4.2	5.0	5.1	6.2	2.8	3.1	3.0	3.6
I2-8	228	234	2.7	7.2	3.1	4.4	4.0	5.7	2.5	2.9	2.8	3.7
I2-9	180	204	3.4	8.6	3.4	4.6	4.4	6.0	2.6	3.0	3.1	3.9
I3-1	168	186	2.3	7.1	2.8	4.3	3.8	5.7	2.5	2.9	2.8	3.7
I3-2	252	288	2.4	6.2	3.0	4.3	3.8	5.5	2.5	2.9	2.7	3.4
I3-3	162	150	3.6	8.6	3.4	4.5	4.5	6.0	2.6	3.0	3.2	4.0
I3-4 (a)	210	204	4.1	7.2	3.6	4.4	4.7	5.7	2.7	2.9	3.2	3.7
I3-4 (b)	198	198	4.2	7.0	3.6	4.3	4.8	5.7	2.7	2.9	3.2	3.7
I3-5 (a)	144	144	4.2	7.8	3.5	4.3	4.8	5.9	2.7	3.0	3.4	3.9
I3-5 (b)	156	162	3.9	8.8	3.4	4.5	4.7	6.1	2.7	3.0	3.3	4.0
I4-1	654	756	5.6	8.5	4.5	5.2	5.3	6.0	2.8	3.0	3.0	3.3
I4-2	714	846	5.8	7.8	4.6	5.1	5.4	5.9	2.9	3.0	3.0	3.2

Table 3: Morphology derived rheological parameters for Profiles in figure 2D. Values are calculated after equations 4,5,6 and 7 for η2, η3, τ1 and τ2, respectively

Profile	*w (m)*	*h (m)*	*Log 10 (η2) Pa s*	*Log 10 (η3) Pa s*	*Log 10 (τ1) Pa*	*Log 10 (τ2) Pa*
A1-1	222	3.9	3.6	4.7	2.7	3.1
A1-2	210	3.0	3.2	4.2	2.6	2.9
A1-3	180	2.4	2.9	3.8	2.5	2.8
A2-1	162	4.6	3.7	5.0	2.8	3.4
A3-1	264	3.8	3.6	4.6	2.7	3.0
A3-2	210	3.2	3.3	4.3	2.6	3.0
A4-1	246	2.5	3.1	3.9	2.5	2.7

Research Highlights for: "**The effect of inflation on the morphology-derived rheological parameters of lava flows and its implications for interpreting remote sensing data. - A case study on the 2014/2015 eruption at Holuhraun, Iceland -**"

1. We present the first comprehensive evaluation of the effect of lava flow inflation on the rheological parameters deduced from lava flow morphology
2. We find that lava flow inflation results in a 2.4 to 17 fold overestimation of apparent viscosity and a 0.7 to 2.4 fold overestimation of yield strength
3. Previous estimates of rheological parameters on Earth and extra-terrestrial bodies may, at best, represent an upper limit, and actual viscosity values of these melts may be significantly lower.
4. The resulting uncertainty in the deduced lava compositions is large and increases for more evolved compositions.
5. Remote sensing and laboratory data are in reasonable agreement with respect to the absolute viscosity that determines the point at which lava flow advance ceases.